JOURNAL OF MATERIALS SCIENCE **40** (2005) 5893–5901

Effect of structure on the creep of open-cell nickel foams

H. S. ZUROB*, Y. BRÉCHET
Laboratoire de Thermodynamique et Physico-Chimie Métallurgiques, Domaine Universitaire, BP 75 38402, St. Martin d'Hères, Cedex, France
E-mail: hatem@zurob.com

A method of constructing the deformation mechanism maps of open-cell foams is proposed. Starting with the deformation behaviour of the constitutive material and taking account of foam geometry, we are able to determine the dominant deformation mechanisms in the foam as a function of the temperature and the applied-stress. The influences of cell-size, cell-strut shape and scales in the microstructure are studied. The model is applied successfully to the experimental results available for open-cell pure nickel foams. © *2005 Springer Science + Business Media, Inc.*

1. Introduction

Recent advances in foaming techniques have made it possible to produce foams with preset densities, cell-sizes and cell-shapes [1]. As foaming techniques continue to improve, it will be possible to manipulate the structure of an increasing number of foams with an increasing level of accuracy. These developments provide new opportunities for creating new materials whose properties are optimized for a given application. In order to take full advantage of this new potential for "materials by design," it is necessary to develop a good understanding of the effect of foam structure on the properties of the foams. To date most studies of the mechanical behaviour of foams have focused on the deformation and failure mechanisms at or near room temperature [2]. At these temperatures, foams deform by elastic bending, elastic buckling and plastic collapse. The relative density is usually the single most important factor that determines the deformation and failure mechanisms. Scale, on the other hand, was shown to have a very weak effect on the mechanical properties, with the exception of fracture [2].

While many of the current applications of foams involve service at or near room temperature, there are several promising applications that would involve service at high temperatures. This is particularly true for metal foams. Potential high-temperature applications of metal foams include catalytic beds, electrodes, heat-exchangers and sandwich structures for thermal insulation and fire barriers [1, 3, 4]. At high temperatures deformation becomes time-dependent giving rise to creep deformation even at small stresses, well below the yield stress. Consequently, it is important to characterize the high temperature deformation behaviour even when the foam is not being used, primarily, for structural purposes. In the present case, we examine the idealized case of the creep deformation of isotropic, open-cell nickel foams. We will examine the effects of the relative density and the strut geometry as well as the effect of scale arising from the grain-size and cell size.

The deformation-mechanisms will be discussed in terms of mechanism maps similar to those developed by Frost and Ashby for bulk metals [5]. The maps identify the dominant deformation mechanism as a function of the applied stress (normalized by the shear modulus) and the homologous temperature. We start by extending the concept of deformation-mechanism maps to foams (Section 2). The maps are used, in Section 3, to examine the influence of the relative density, strut-geometry and scale on the deformation mechanism. In Section 4, the accuracy of the maps is verified against some of the existing experimental data on Ni foams.

2. Construction of deformation mechanism maps

Steady-state conditions are often reached during constant load (creep) and constant strain-rate tests of polycrystalline materials at high temperatures ($T > 0.5\ T_m$ where T_m is the melting temperature). When steady-state is reached during creep loading, the solid continues to deform at a constant strain-rate with no significant increase in the applied stress. The steady-state strain rate is then a function of only the deformation temperature and the applied stress. Frost and Ashby [5] attributed a strain-rate to each of the deformation mechanisms acting at a given stress and temperature. They then defined the dominant deformation mechanism as the one making the largest contribution to the total strain-rate. In this way it is possible to identify in

*Author to whom all correspondence should be addressed.
1438-2377
DOI: 10.1007/s10853-005-5031-8

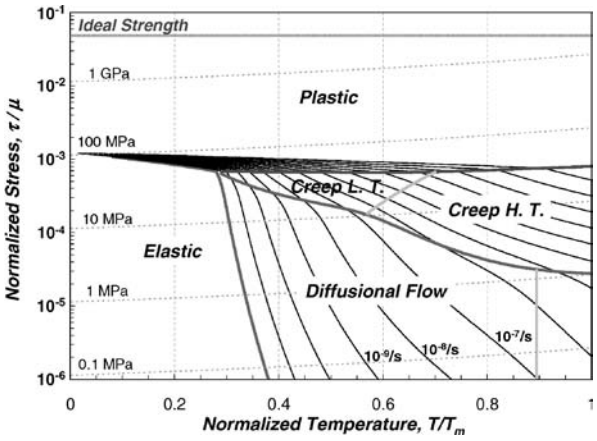

Figure 1 Deformation mechanism map of solid Ni having a grain size of 30 μm.

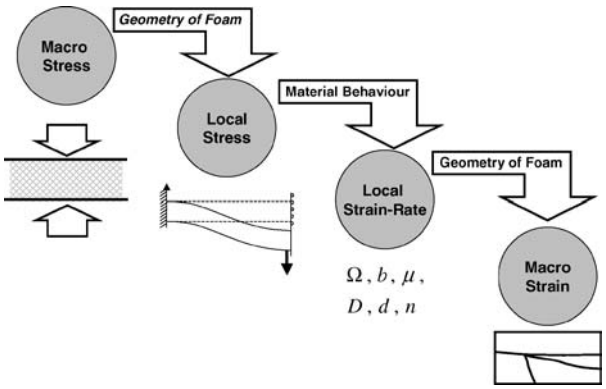

Figure 2 Illustration of the approach used to calculate the mechanism maps of foams. The correlation of global and local quantities involves knowledge of the foam geometry.

temperature-stress space the conditions over which a given deformation mechanism dominates.

The deformation mechanism map for pure bulk nickel with a grain-size of 30 μm is shown in Fig. 1. The map was plotted in terms of the normalized stress (τ/μ, where τ is the shear stress and μ is the shear modulus) vs. the homologous temperature (T/T_m), with contours of the total shear strain-rate ($\dot{\gamma}$). Four fields appear on the map. Each field is dominated by one the following deformation mechanisms:

1. *Elastic deformation:* At low temperatures and for small stresses, plastic deformation is negligible and the material behaviour is essentially elastic. In this work, the material behaviour is considered elastic when the steady-state strain rate is less than 10^{-12}/sec.

2. *Power-law creep:* At high temperatures ($T > 0.3T_m$) dislocations can overcome obstacles by climb. The rate of deformation is then controlled by the thermally-activated climb of dislocations. A power-law function is then found to provide a reasonable description of the stress dependence of the strain rate. The power-law creep field is subdivided into two regions corresponding to low and high temperature behaviour. In the first case, transport occurs mainly by pipe-diffusion, while in the second case it occurs mainly by volume diffusion [5].

3. *Diffusional flow:* Stress changes the chemical potential of atoms on surfaces and grain-boundaries. The presence of a shear stress will change the chemical potential of some grain-boundaries more than others. As a result, potential gradients are created and atoms diffuse in response to these [6]. A strain rate could be attributed to this diffusional flow. The resulting field on the deformation-mechanism map is subdivided into two regions; the first corresponds to the case in which transport is dominated by boundary diffusion (low temperature) and the other corresponds to bulk diffusion (high temperature) [5].

4. *Low temperature plasticity:* At low temperatures nickel deforms by dislocation glide. The rate of deformation is obstacle-limited [5]. Stress assists the dislocations at overcoming the activation energy barrier in order to escape the obstacle. Consequently, the strain-rate is an exponential function of the stress. A steady-state strain-rate is rarely achieved at low-temperature. As a result, the maps are constructed for conditions of constant structure (constant stress). This is to say, we calculate the yield stress for a given temperature and strain-rate [5].

Essentially the same deformation processes are expected to appear on the mechanism maps of nickel foams. However, the applied stress at the macroscopic level generates a local stress at the level of the cell elements, which is the relevant driving force for plastic flow. As a consequence, the positions of the various field-boundaries will change as a function of the foam structure. In order to construct the deformation mechanism maps of the foam we adopt the approach shown in Fig. 2. To start the global applied stress is related to the local stress acting on the struts of the foam. The effect of this local stress on the deformation of the strut material is then analyzed and a local strain rate is calculated using the properties of the bulk material (e.g. diffusion coefficient, elastic modulus, creep exponent. . . etc). Finally the geometry of the foam is used to relate the local strain-rate to the observed global strain rate. Knowledge of foam geometry is essential for the steps in which we relate the global and local quantities. However, a complete analysis of this geometrical problem is often too complicated. As a result, we adopt the approach of Gibson and Ashby [2]. In this approach the global stress and strain-rate are related to their local counterparts by scaling constants which are determined by fitting existing experimental data.

In Sections 2.1–2.4 we discuss in detail the manner in which the strain-rate is related to the applied stress and temperature for each of the above deformation mechanisms. The foams are modelled using the unit cell proposed by Gibson and Ashby [2]. The cell is a cube of side l and strut width t as shown in Fig. 3. Adjoining cells are staggered so that their members meet at their midpoints. While this unit-cell differs from those observed in real foams, useful results can still be obtained by using the experimentally determined scaling constant, as described earlier.

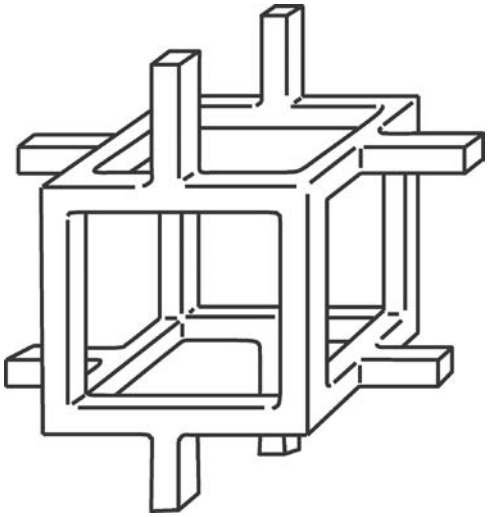

Figure 3 Illustration of Gibson-Ashby unit cell [2] which is being used to describe the foam structure. The cube edge length is l and the strut thickness is t_w.

2.1. Elastic properties of foams

When a shear stress of τ is applied to the foam, the beams respond by bending. For a strut of length l, the deflection, δ, is proportional to Fl^3/E_sI, where E_s is the Young modulus of the strut material and I is the second moment of area of the member. Assuming that $I \propto t^4$, $F \propto \tau l^2$, $\varepsilon \propto \delta/l$ and $\rho^*/\rho^S \propto (t/l)^2$, Gibson and Ashby [2] arrive at the expression:

$$\frac{\mu^*}{E^S} \approx C_1 \left(\frac{\rho^*}{\rho^S}\right)^2 \tag{1}$$

where μ^* and ρ^* are, respectively, the shear modulus and density of the foam. ρ^S is the density of the solid.[1] In the above approach, all of the geometric details of the problem were incorporated into the constant C_1. Gibson and Ashby [2] estimated the value of C_1 by fitting the existing experimental data for a broad range of foams. Using a similar analysis, the value of the elastic modulus of the foam can be derived. Equation 2 summarizes the values of the elastic constants as obtained by [2]:

$$\frac{\mu^*}{E^S} \approx \frac{3}{8}\left(\frac{\rho^*}{\rho^S}\right)^2 \tag{2a}$$

$$\frac{E^*}{E^S} \approx \left(\frac{\rho^*}{\rho^S}\right)^2 \tag{2b}$$

$$\upsilon^* \approx \frac{1}{3} \tag{2c}$$

In order to analyze the effect of strut geometry on the elastic behaviour of foams, we repeated the above analysis for solid and hollow struts of square, circular and triangular cross sections as shown in Fig. 4. The results are summarized in Table I below. It should be pointed out that the value of C_1 was kept equal to 1 for all of the various geometries. As such, the differences between the various expressions are purely due to the effect of beam geometry on the second moment of area, I. When the various moduli are compared for a constant beam cross section, it is found that the modulus increases in the order: circle, square, triangle.

TABLE I Elastic moduli of foams having the strut geometries shown in Fig. 4

Square	Circle	Triangle
$\left(\frac{t_w^4-t_v^4}{l^4}\right)E^S$	$\frac{3\pi}{16}\left(\frac{t_w^4-t_v^4}{l^4}\right)E^S$	$\frac{\sqrt{3}}{8}\left(\frac{t_w^4-t_i^4}{l^4}\right)E^S$

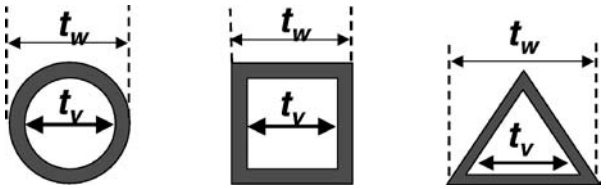

Figure 4 The various strut cross-sections which are to be considered in this work.

2.2. Low temperature plasticity

When yielding takes place in compressively loaded metallic foam, plastic hinges develop and the foam collapses plastically. Under these circumstances, it is not possible to relate the strain-rate, temperature and applied-stress using the steady-state formalism [5]. Our approach is then to identify the stress at which plastic collapse occurs at a given temperature and for a given strain-rate. Strain-rate contours are, therefore, not meaningful for stresses larger than this collapse stress.

For the present case in which glide is controlled by forest dislocation obstacles, the yield stress is related to the strain-rate and temperature by the standard equation [5]:

$$\dot{\gamma}^* = 10^{12}\left(\frac{\tau^*}{\mu}\right)^2 \exp\left(\left(\frac{-\Delta F}{kT}\right)\left(1-\frac{\tau^*}{\tau_{0K}^*}\right)\right) \tag{3a}$$

In this equation, τ is the shear stress and k is Boltzmann's constant. The activation energy, ΔF, is that needed to overcome an obstacle without the assistance of stress. Following Frost and Ashby [5], this quantity is estimated as $\Delta F \approx 0.5\mu_0^S b^3 = 3.8\,\text{eV}$. The yield stress of the foam at 0 K, τ_{0K}^*, depends on the density and geometry of the foam. We approximate, τ_{0K}^*, using a modification[2] of the result derived by Gibson and

[1] Throughout this work we will follow the convention in which an asterisk is used to denote foam properties while a superscript, S, is used to identify the properties of the solid.

[2] In [2] the result is stated as: $\sigma^* = 0.3\sigma_{ys}^S(\rho^*/\rho_s)^{1.5}$ For cubic cells with square struts, the relative density is $3t_w^2/l^2$ In addition, $H = t_w^3/4$. Therefore, the proportionality constant in Equation 3b becomes $(0.3)(4)(3)^{1.5} = 6.24$.

TABLE II Values of $H = \int y dA$ for the various strut cross-sections shown in Fig. 4

Square	Circle	Triangle
$\frac{1}{4}(t_w^3 - t_i^3)$	$\frac{1}{6}(t_w^3 - t_i^3)$	$\frac{2}{27}(t_w^3 - t_i^3)$

Ashby [2]:

$$\tau_{0K}^{*} \approx 6.24\tau_{0K}^{S}\left(\frac{H}{l^3}\right) \tag{3b}$$

where τ_{0K}^{S} is the yield stress of the solid at 0 K. Following [5], τ_{0K}^{S} is estimated as $\mu b/l_s$, l_s being the spacing of the forest dislocation obstacles. For well-annealed samples, the value of l_s is of the order of 10^{-7} m. As for the moment, H, in Equation 3b it is defined as $\int y dA$, where y is the distance measured from the neutral axis. Table II lists the values of H for the various strut geometries shown in Fig. 4.

To conclude the present discussion it is important to consider the case in which the foam is loaded in tension. To a first approximation, the foam is expected to yield by the same mechanism in both tension and compression [2]. The main difference concerns the post-yield behaviour. In the case of tensile loading the beams will rotate and gradually align in the direction of the applied load. This will reduce the bending moment on the beams and, gradually, stretching will become the dominant deformation mechanism. For the present analysis we are only interested in the onset of yielding and as such, the equations derived above can still be used.

2.3. Power-law creep

The power-law creep rate, $\dot{\gamma}$, of a beam which is loaded along its axis is given by the simple constitutive law [5]:

$$\dot{\gamma} = \dot{\gamma}_o\left(\frac{\tau}{\tau_o}\right)^n \tag{4a}$$

The constants, $\dot{\gamma}$, τ_o and n, are material-dependent. In the case of nickel, the creep exponent, n, is equal to 4.6, τ_o is approximately equal to the shear modulus, μ^S, and $\dot{\gamma}_o$ is given by [5]:

$$\dot{\gamma}_o = (3 \times 10^{-6})(\sqrt{3})^{n+1}\frac{D_{\text{eff}}\mu b}{kT} \tag{4b}$$

The effective diffusion coefficient, D_{eff}, takes account of the fact that mass-transfer can take place by pipe-diffusion as well as bulk diffusion. The value of D_{eff} is then a weighted average of the two contributions [5]:

$$D_{\text{eff}} = D_v + Pa_cD_c \tag{4c}$$

The constants, D_v and D_c, are the bulk and pipe diffusion coefficients, respectively, and a_c is the cross-sectional area of the pipe diffusion path. The values of these constants, as well as others, are taken from the review by Frost and Ashby [5]. The dislocation density, P, in Equation 4c could also be expressed in terms of τ^2. Consequently, an effective creep exponent of $n + 2$ is expected at low temperatures where mass transfer is controlled by pipe diffusion. At high temperatures, mass transfer is controlled by bulk diffusion and the creep exponent is n. Use of the present formalism leads to smooth transition between the low and high temperature behaviours [5].

Analysis of the creep of foams is more complex than that described above because it involves the creep of a beam in bending as shown in Fig. 5. This problem was analyzed by Andrew *et al.* [3] who arrived at the general result that:

$$\dot{\delta} = \left(\frac{1}{n+2}\right)\frac{\dot{\kappa}_o F^n l^{n+2}}{M_o^n 2^{n+1}} \tag{5}$$

In this equation $\dot{\delta}$ is the beam deflection rate, F is the applied force and $\dot{\kappa}_o$ is equal to $2\dot{\gamma}_o/t_w$. M_o is a constant whose value depends on the cross-section of the beam. A summary of the value of M_o for square, circular and triangular beams is provided in Table III, below.

The global creep rate of the foam, $\dot{\gamma}^*$, is related to the deflection rate, $\dot{\delta}$, and the globally applied stress, τ^*, by two scaling constants, C_2 and C_3. The general foam creep equation is then given by:

$$\frac{\dot{\gamma}^*}{\dot{\gamma}_o} = \frac{2C_2(C_3\tau^*)l_c^{3(n+1)}}{(n+2)(2^{n+1})M_o^n t_w} \tag{6}$$

Starting with this equation and fitting existing experimental data in the limits of $n = \infty$ and $n = 1$, Andrews *et al.* [3] obtained $C_2 = 0.6$ and $C_3 = 1.7$.

2.4. Diffusional creep:

The rate of diffusional flow in bulk materials is described by the equation [6]:

$$\dot{\gamma} = f\frac{\Omega D_{\text{eff}}}{kT}\tau \tag{7}$$

where Ω is the atomic volume and D_{eff} is an effective diffusion coefficient which takes into account the contributions of bulk and boundary diffusion. Mathematically, Equation 7 is a special case of Equation 4, with n =1, $\dot{\gamma}_0 = f D_{\text{eff}}$ and $\tau_0 = kT/\Omega$. Consequently, the results which were derived in Section 2.3 for the power-law creep of foams could be used to describe the diffusional flow of foams, provided that the appropriate substitutions are made.

An important feature of diffusional flow is scale dependence; in Equation 7, f is a function whose value is determined mainly by the grain-size. For the case in which the grain size is much smaller than the strut size, f takes the value of $\sim 40/d^2$ [6]. When the grain-size is comparable to the beam size, the value of f becomes dependent on the geometry of the specimen as shown in

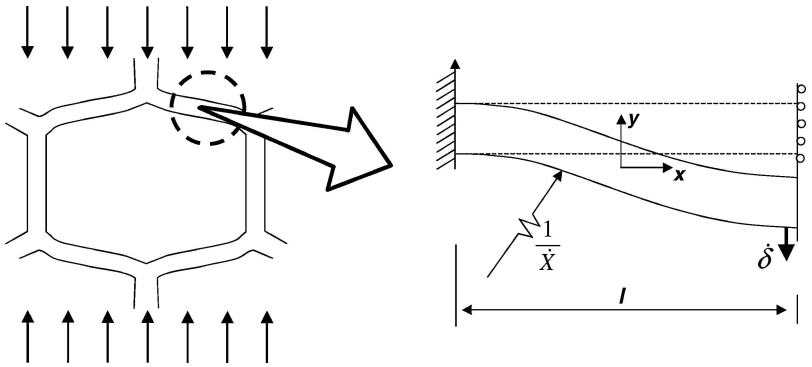

Figure 5 Illustration of the geometry of the beam bending problem considered by Andrews *et al*. [3].

Table IV. In most foams, the grain-size is comparable to the strut thickness. Under these circumstances, we have modelled solid struts as wires of diameter t_w and grain-size d. Hollow struts were modelled as foils having the same thickness as the strut wall. The value of the effective diffusion coefficient is also dependent on the geometry when the grain size is comparable to the strut size and the appropriate values of D_{eff} are shown in Table IV.

3. Modelling results

The equations derived in Section 2 contain all of the information needed to construct the deformation mechanism maps for open-cell nickel foams. In order to describe the foam completely, it is necessary to identify the relative density, the cell size, the strut geometry (shape & void size) and the grain-size. Fig. 6 is the deformation mechanism map of a foam having a relative-density of 20%, cell-size (edge length) of 400 μm and a grain-size of 20 μm. The struts of this foam were assumed to be full with a square-cross section of edge length 100 μm. The fields which appear on the foam map are the same as those appearing in the bulk material map. The main difference is that the applied stresses are much smaller than those encountered in the bulk materials. This is to be expected since the stresses acting on the struts are larger than the applied stress by a factor of the order of $1/(\rho^*/\rho^S)$.

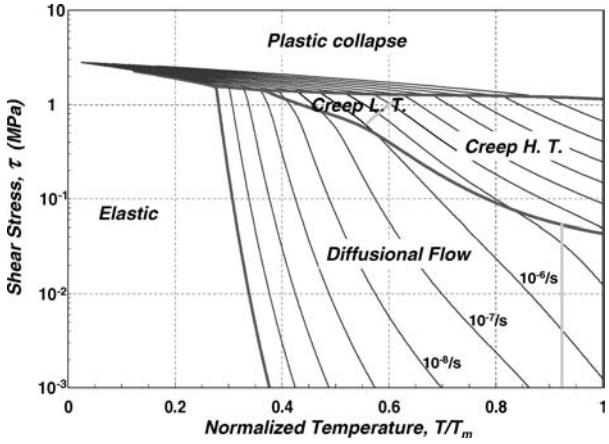

Figure 6 Example of the deformation mechanism map of Ni-foams. In this example, the relative density is 20%, the cell-size is 400 μm and the grain size is 20 μm. The struts are assumed to be solid with square-cross section.

In what follows, we examine the effects of the relative density (Section 3.1), strut geometry (Section 3.2) and scale (Section 3.3) on the deformation of open-cell nickel foams.

TABLE III Values of the constant M_0 for the various strut cross-sections shown in Fig. 4. Expressions for the square and triangular cross-sections allow for both solid and hollow struts, where as, the expression for the circular cross-section applies only to solid struts

	M_o
Square	$\frac{\tau_o(t_w^{(3n+1)/n}-t_v^{(3n+1)/n})}{2(2n+1)t_w^{1/n}}$
Circle	$\frac{\sqrt{\pi}\tau_o\Gamma\left(\frac{2n+1}{2n}\right)}{8\Gamma\left(\frac{5n+1}{2n}\right)}$, where $\Gamma(m)=\int_0^\infty \exp(-z)\,z^{m-1}dz$
Triangle	$\frac{\tau_o n((8n(3^{1/(2n)}t)+3^{(1/2n)/(2n)}+8n(6)^{1/n}(3)^{-1/(2n)})(t_w^{(1+3n)/n}-t_v^{(1+3n)/n}))}{36(6n^2+5n+1)(3)^{1/n}t_w^{1/n}}$

3.1. Effect of relative density

Foam properties are strongly dependent on the relative-density. In Section 2 it was shown that the elastic modulus varies as $(\rho^*/\rho^S)^2$ while the yield stress varies as $(\rho^*/\rho^S)^{1.5}$. It is the creep rate, however, which shows the strongest dependence on the relative density. In the simplest case of open-cell foam with solid-struts, the creep rate varies as $(\rho^*/\rho^S)^{-(3n+1)/2}$. Consequently, the ratio of the creep rate of a foam of relative density of 2% to that of a foam with a relative density of 20% could be as large as 10^8.

TABLE IV Summary of the quantities needed to calculate the diffusional flow rate for various sample geometries and grain-sizes

Sample geometry	Grain geometry	f	D_{eff}
Any shape, for e.g. sphere of radius a	Sphere of diameter $d \ll a$	$\frac{40}{d^2}$ [6]	$D_v + \frac{3.5}{d}a_b D_b$
Foil of thickness a	Square array with side length $d > a$	$\frac{22.4}{ad}$ [6]	$D_v + \frac{1.6}{a}a_b D_b$
Wire of diameter a	Cylinder of length $d > a$	$\frac{37.1}{ad}$ [6]	$\approx D_v$

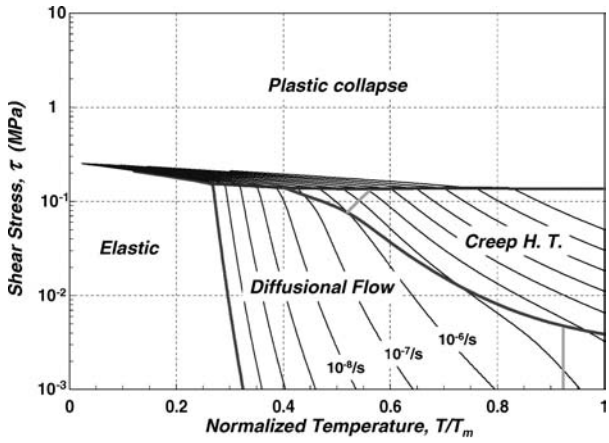

Figure 7 Deformation map for a foam having a relative density of 4%, the cell-size of 400 μm and the grain size is 20 μm. As before, the struts are solid with a square-cross section.

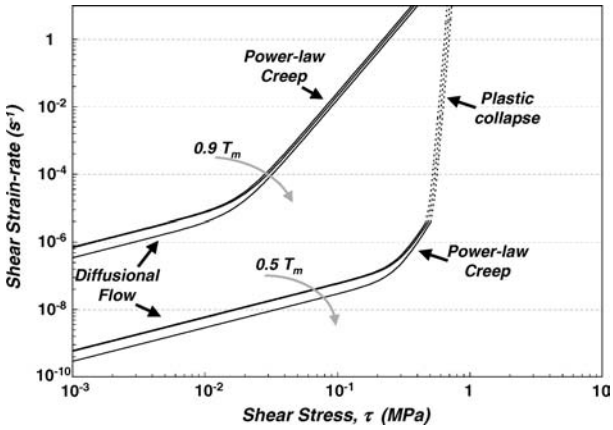

Figure 9 Effect of the strut shape on strain-rate of the foam at 0.5 and 0.9 T_m. The relative density is 10%, the cell size is 400 μm and the grain size is 20 μm. The shape of the strut cross-section changes from circular to square to triangular in the direction of the arrows.

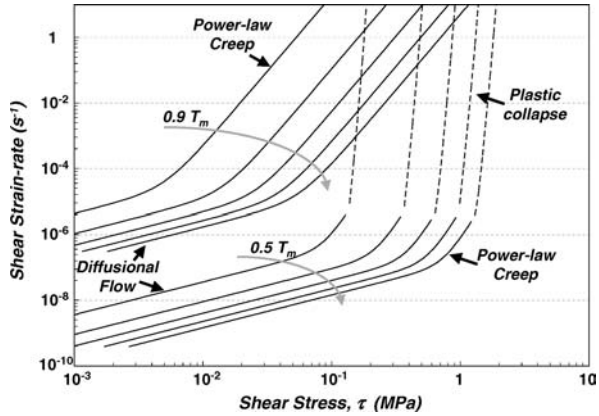

Figure 8 Effect of the relative density on the strain-rate of the foam at 0.5 and 0.9 T_m. The cell size is 400 μm, the struts are square and grain size is 20 μm. The relative density increases in the direction of the arrow in the order 4, 8, 12, 16 and 20%.

The influence of the relative density on mechanical properties is clearly illustrated in Figs 7 and 8. Fig. 7 is the deformation mechanism map of a foam having a relative density of 4%. It should be compared to Fig. 6, which is the mechanism map for a foam with a relative density of 20%. The effect of the relative density on the yield stress is immediately clear. It is also noticeable that the regime of low-temperature creep is wider in the foam with the higher density. This is attributed to the larger stresses which act on the high density foam and consequently lead to higher dislocation density. The effect of the relative density on the creep rate is more clearly shown in Fig. 8. In this figure the steady-state strain-rate is plotted against the applied stress for foams with densities between 4 and 20%. The effect is most remarkable in the power-law regime where n is 4.6. A smaller, but still significant, effect is encountered in the diffusional flow regime where n is 1.

3.2. Effect of strut geometry

The bending resistance of a beam of length l and cross-sectional area A is determined by the second moment of the cross-section, I. We begin by comparing the mechanical behaviours of foams having non-hollow struts with square, circular and triangular cross-sections. Fig. 9 shows the effect of the strut shape on the creep rate at 0.5 and 0.9 T_m. The triangular and circular cross-sections appear to offer, respectively, the maximum and minimum resistance to bending among the shapes considered. The difference between the creep rates for the various geometries is, however, relatively small, typically, of the order of a factor of 3 or less.

In the case of hollow struts the system acquires and additional degree of freedom. It is now possible to vary the ratio of the void-size to the strut-size (t_v/t_w) at a constant relative density. In Fig. 10, the strain-rate is plotted as a function of the applied stress for increasing values of t_v/t_w. As expected, the creep rate decreases as the value of t_v/t_w increases. This follows from the fact that the second moment of the cross-section increases with t_v/t_w. An important implication of the present result is that the creep rate can be reduced by as much as a factor of 100 without changing the relative density. Caution should be exercised, however, because as t_v/t_w increases, the walls of the strut become increasingly thinner and the strut walls become increasingly susceptible to plastic buckling. The important point, then, is that the bending resistance of the foam can

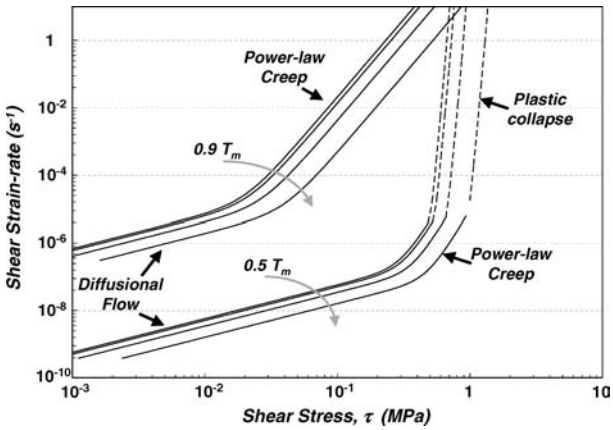

Figure 10 Effect of the strut shape on strain-rate of the foam at 0.5 and 0.9T_m. The relative density is 10%, the cell size is 400 μm and the grain size is 20 μm. The struts are hollow with a square cross section. The ratio t_v/t_w increases in the direction of the arrow in the order: 0, 0.25, 0.50 and 0.75.

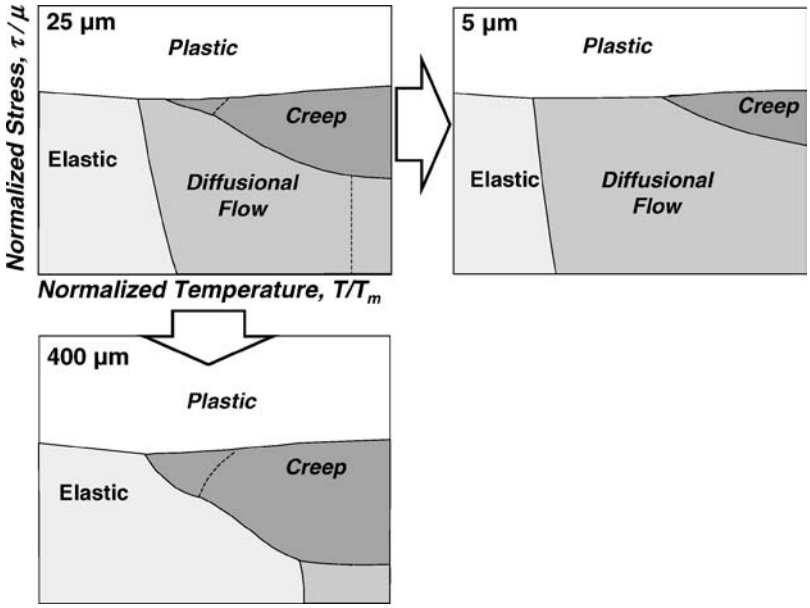

Figure 11 Effect of grain size on the deformation mechanism map of 10% and cell-size of 400 μm. The struts are solid with a circular cross-section. The grain size is indicated at the top left-hand corner of each map.

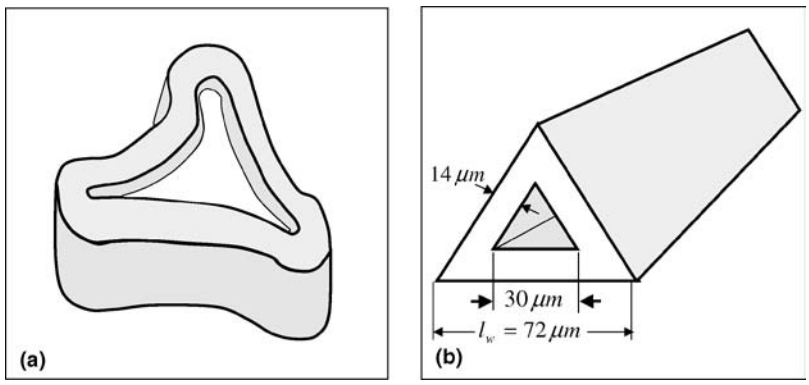

Figure 12 (a) Schematic diagram of the strut geometry typically observed in the SEM. (b) Idealized strut geometry used to model the behaviour of the 3.5% foam.

be optimized, without changing the relative density, by controlling the value of t_v/t_w.

3.3. Effect of scale

In this section the effect of scale on the deformation behaviour is discussed in terms of the cell-size, l, and the grain-size, d. Starting with the cell-size, we observe that the deformation behaviour is unaffected by changes in l, provided that the relative density and the slenderness (t_v/t_w) are kept constant. This result is in agreement with the analysis of Gibson and Ashby for solid-strut foams [2].

We next turn our attention to the effect of grain-size on deformation. As mentioned in Section 2, the rate of diffusional flow is inversely proportional to the grain size to the second or third power. Consequently, decreasing the grain-size will expand the diffusional flow field at the expense of the other fields. In addition, decreasing the grain-size will increase the contribution that grain-boundary diffusion makes to mass transport and this will expand the region of low-temperature diffusional flow at the expense of the high-temperature region. These changes are shown in Fig. 11, in which three grain sizes are considered. As discussed in Section 2.4, the appropriate equations for diffusional flow should be chosen with care when the grain-size is comparable to, or greater than, the width of the strut. In the above example, the struts have a circular cross section with a diameter of 80 μm. The equations for diffusional flow in wires were used to describe the case where d is 400 μm, i.e. $d \gg t_w$.

4. Comparison with experimental data

Most of the existing experimental data on nickel-foams concerns their mechanical behaviour near room temperature. Data on the high temperature behaviour of these foams is very limited. In the present section, we make use of the recent results of Goussery [4] on the creep of nickel foams to verify the accuracy of our mechanism maps. The foams considered had relative densities of 2.9, 3.5, 6.1 and 7.2%. The first three foams were tested at 500, 600 and 700°C, while the last was tested only at 600 °C. The above temperatures correspond, respectively, to 0.45, 0.51, 0.56 T_m.

Scanning electron microscopy (SEM) observations by Goussery [4] showed that the cells were slightly elongated spheres with a diameter of ~500 μm. The struts were hollow and had the geometry shown in Fig. 12a. In our calculations, we approximated the strut cross-section as being triangular with a void size of

TABLE V Comparison between the predicted and experimentally measured [4] strain-rates in the 3.5% foam. See text for details

Temperature (°C) & shear-stress (MPa)	Measured shear strain-rate (s^{-1})	Calculated shear strain-rate (s^{-1})	Ratio (Measured/Calc.)
500, 0.127	2.1 E-7	3.3 E-7	0.63
500, 0.161	2.4 E-7	1.0 E-6	0.24
500, 0.179	9.7 E-6	1.8 E-6	0.54
500, 0.202	3.8 E-6	3.8 E-6	1.01
600, 0.127	1.0 E-5	5.6 E-6	1.80
600, 0.161	2.8 E-5	2.2 E-5	1.24
600, 0.179	3.8 E-4	4.2 E-4	0.91
600, 0.202	2.1 E-4	9.0 E-5	2.31
700, 0.087	3.3 E-5	1.5 E-5	2.22
700, 0.115	6.2 E-5	5.9 E-5	1.06
700, 0.127	1.6 E-4	9.8 E-5	1.61

30 μm. The thickness of the strut wall depends on the density of the foam considered. Fig. 12b shows the geometry used for modeling the foam with a relative density of 3.5%. The grain size was taken to be 10 μm which is of the order of the strut wall thickness, in agreement with the experimental observations [4]. As for the cell geometry, it was modelled as being cubic (Fig. 3) with side length of 400 μm. This value is chosen so as to produce the same volume as a sphere of diameter 500 μm. Finally, the obstacle spacing, l_s, was estimated from experimental measurements of the yield-stress at room-temperature.

Table V compares the predicted and the experimentally measured values of the strain-rate of the 3.5% foam. In most cases, the results of the model are within a factor of 2 of the experimental results. The agreement is remarkable considering that many of the physical quantities that enter into the model are only know to within a factor of 2 or 3. Comparison between the model's predictions and the experimental data on the other three foams leads to agreement within a factor of 2, 70% of the time. The present results support the creditability of the model, especially considering that no adjustable-parameters have been used to fit the present experimental data.

In Fig. 13, the experimental data for the 3.5% foam is superimposed on the computed deformation mechanism map of the foam. It is interesting to note that the experiments were carried out near the border region between diffusional flow and power-law creep. As such, the creep exponents derived from the experimental data are expected to show intermediate values between $n = 1$, for diffusional flow and $n = 4.6 + 2$ for low-temperature creep. This is indeed the case as the experimentally measured exponents were between 3.7 and 6.

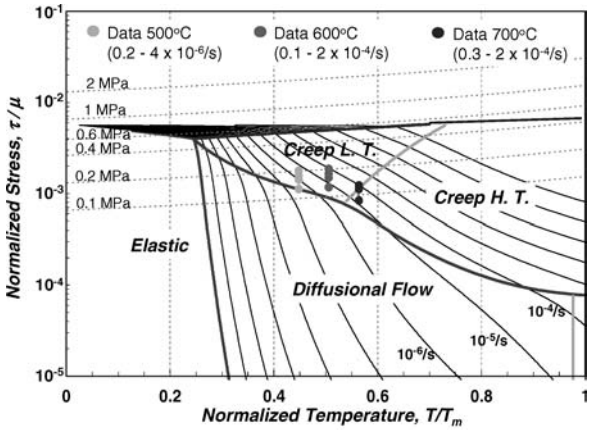

Figure 13 The placement of the experimental data of [4] on the deformation mechanism map for the 3.5% foam.

5. Summary and future work

The hot-deformation behaviour of nickel foams was investigated using the approach of deformation-mechanism maps. Using these maps we examined the effect of foam structure on the dominant deformation mechanism and the observed strain-rate. The results could be briefly summarized as follows:

1. The relative density has the greatest influence on the deformation behaviour of foams. The most dramatic effect is observed in relation to the rate of power-law creep. This rate could increase by as much as 8 orders of magnitude when the relative density is reduced by a single order of magnitude.

2. The shape of the strut had a relatively minor effect on the deformation behaviour. The creep rate of struts having a triangular cross-section was approximately twice that of struts having a circular cross section of the same area.

3. Variation of the ratio of void-size to the strut size (t_v/t_w) in hollow-strut beams can change the creep rate by up to two orders of magnitude. This presents an opportunity for manipulating the properties of the foam without varying the relative density.

4. The size of the foam cells does not affect the deformation mechanism, provided that the relative density and the slenderness (t_v/t_w) are kept constant.

5. Decreasing the grain size will enhance the rate of diffusional flow and consequently, expand this field at the expense of the other fields in the map.

Comparison between the predicted and experimentally measured strain-rates confirms the accuracy of the model. In general the predicted strain-rates are within a factor of 2 or less of the measured values. Having established the accuracy of the present approach, it is now possible to use the deformation mechanism maps as a design tool for planning future

experimental work on the hot-deformation of foams. With the aid of the maps it is very simple to identify the experimental conditions under which a certain mechanism is expected to dominate. Experiments could then be carried out to understand the mechanism of interest in detail. Alternatively, the maps could be used to identify and investigate those conditions for which a transition in the deformation mechanism is expected.

Acknowledgments

HSZ gratefully acknowledges the financial support of the Natural Science and Engineering Research Council of Canada in the form of a post doctoral fellowship.

References

1. V. PASERIN, S. MARCUSON, J. SHU and D. S. WILKINSON, *Adv. Eng. Mater.* **6** (2004) 454.
2. L. J. GIBSON and M. F. ASHBY, in "Cellular Solids: Structure and Properties" (Cambridge University Press, Cambridge, 1999).
3. E. W. ANDREWS, L. J. GIBSON and M. F. ASHBY, *Acta Mater.* **47** (1999) 2853.
4. V. GOUSSERY-VAFIADES, in "Caractérisations Microstructurale et Mécanique de Mousses de Nickel à Cellules Ouvertes pour Batteries de Véhicules Hybrides" (Ph.D. Thesis, Ecole des Mines de Paris, 2004).
5. H. J. FROST and M. F. ASHBY, in "Deformation-Mechanism Maps: The Plasticity and Creep of Metals and Ceramics" (Pergamon Press, Oxford, 1982).
6. H. JONES, *Mater. Sci. Eng.* **4** (1969) 106.

Received December 2004
and accepted April 2005